CHINESE OPTICS LETTERS

Vol. 20, No. 3 | March 2022

AgGeSbTe thin film as a negative heat-mode resist for dry lithography

Xingwang Chen (陈兴旺)[1,†], Lei Chen (陈 雷)[1,†], Ying Wang (王 莹)[1], Tao Wei (魏 涛)[1,2*], Jing Hu (胡 敬)[1], Miao Cheng (程 淼)[1], Qianqian Liu (刘倩倩)[1**], Wanfei Li (李宛飞)[1], Yun Ling (凌 云)[1,3], and Bo Liu (刘 波)[1***]

[1] Suzhou Key Laboratory for Nanophotonic and Nanoelectronic Materials and Its Devices, School of Materials Science and Engineering, Suzhou University of Science and Technology, Suzhou 215009, China

[2] State Key Laboratory of Functional Materials for Informatics, Shanghai Institute of Microsystem and Information Technology, Chinese Academy of Sciences, Shanghai 200050, China

[3] School of Electronic & Information Engineering, Suzhou University of Science and Technology, Suzhou 215009, China

*Corresponding author: weitao@usts.edu.cn

**Corresponding author: liuqianqian@usts.edu.cn

***Corresponding author: liubo@mail.usts.edu.cn

Received November 17, 2021 | Accepted December 29, 2021 | Posted Online January 21, 2022

An AgGeSbTe thin film is proposed as a negative heat-mode resist for dry lithography. It possesses high etching selectivity with the etching rate difference of as high as 62 nm/min in CHF_3/O_2 mixed gases. The etched sidewall is steep without the obvious lateral corrosion. The lithographic characteristics and underlying physical mechanisms are analyzed. Besides, results of X-ray diffraction, Raman spectroscopy, and X-ray photoelectron spectroscopy further indicate that laser irradiation causes the formation of Ge, Sb, and AgTe crystals, which is the basis of etching selectivity. In addition, the etching selectivity of Si to AgGeSbTe resist is as high as 19 at SF_6/Ar mixed gases, possessing good etching resistance. It is believed that the AgGeSbTe thin film is a promising heat-mode resist for dry lithography.

Keywords: thin film; heat-mode resist; lithography.

DOI: 10.3788/COL202220.031601

1. Introduction

Laser heat-mode lithography has a promising prospect in the optoelectronic region due to its high resolution, low cost, facile fabrication process, and so forth[1]. Heat-mode lithography involves resist and the lithographic method. So far, different lithographic techniques have been proposed including scanning probe lithography[2], electron-beam lithography[3], and direct laser writing[4]. Among others, direct laser writing is promising in micro/nano fabrications because of its relatively high speed and facile operation (that is, operated in air)[4–7].

On the other hand, various heat-mode resists have been found for lithography such as organic polymers[8], metallic alloys[9,10], and chalcogenide phase-change materials[11–13]. Among others, chalcogenide material has recently been widely investigated as a heat-mode resist due to its low surface roughness, easy preparation, phase-change threshold effect, and atom-scale resolution[1]. Currently, nanoscale feature size (smaller than 50 nm) can be achieved in chalcogenide heat-mode resist[14]. Moreover, high density (the duty cycle of 1:1), multiscale (the minimum size varying from 90 nm to 2.7 μm), and arbitrary patterns have also been realized[15]. Besides, chalcogenide heat-mode resist also exhibits high etching resistance, and the patterns can be transferred onto various substrates, including silicon[11,16], fused silica glass[12,17], GaAs[18], etc. These researches have greatly promoted the development of laser lithography.

However, wet development is adopted in heat-mode lithography, which readily results in the undercut of resist and, therefore, the pattern collapse[19]. At the same time, wet development will also readily cause resist swelling, influencing the pattern fidelity. Fortunately, dry development of heat-mode resist has recently been proposed to effectively address the above-mentioned issues[20], where $CrSb_2Te$ film has been used as a positive heat-mode resist at CHF_3 and O_2 gas mixtures. The etching mechanism of the resist is ascribed to the occurrence of Sb and $CrSb_2Te_3$ phases after laser exposure and, thus, the readily broken Sb phase during the dry development. However, as far as we know, negative heat-mode resist has yet to be reported for dry development. Here, an AgGeSbTe thin film is proposed as a negative resist for dry lithography. The lithographic characteristics, etching resistance, and underlying mechanisms are investigated.

2. Experimental Details

AgGeSbTe films with the thickness of 250 nm were prepared onto silicon substrates according to the co-sputtering technique with Ag and $Ge_2Sb_2Te_5$ alloy targets. Before sputtering, the chamber pressure reached 7×10^{-4} Pa. The powers of Ag and $Ge_2Sb_2Te_5$ targets were 15 W and 80 W, respectively, along with the working pressure of 0.8 Pa and the time of 5 min at the sputtering rate of 50 nm/min. The home-built direct laser writing instrument was used to expose the prepared AgGeSbTe thin films with 658 nm as the laser wavelength, spot diameter of 3 μm, and the exposed energy varying from 0.4×10^3 mJ/cm^2 to 1.4×10^3 mJ/cm^2. A reactive ion etching instrument equipped with SF_6, CF_4, CHF_3, Ar, and O_2 gases was employed to achieve dry development of the exposed samples and the etching of the Si substrate, where the type was Oxford PlasmaPro 80, United Kingdom. In this work, CHF_3 and O_2 were adopted for dry development via the optimal experimental parameters, while SF_6 and Ar gases were used for Si etching.

Atomic force microscopy (AFM) was utilized to determine the sample height information, where the instrument type was Nanosurf Core AFM, Switzerland. The scanning electron microscope (SEM, JSM-IT100) and transmission electron microscope (TEM, Tecnai G2 F20 S-TWIN) were used to observe cross-section profiles and surface morphologies. The composition ratio of AgGeSbTe resist was characterized via energy-dispersive X-ray spectroscopy (EDS), where the atomic fractions of Ag, Ge, Sb, and Te were 34.9%, 20.4%, 13.9%, and 30.8%, respectively. The crystallization temperature of AgGeSbTe was determined via the dependence of resistance on temperature measured by LINKAM HFS600E-PB4 hot stage. The crystal structures of the exposed samples were analyzed by an X-ray diffractometer of Bruker advance D8, Germany. The bonding environments of resists were measured according to the Raman spectroscopy (HORIBA LabRAM HR Evolution, laser wavelength of 532 nm) and X-ray photoelectron spectroscopy (XPS, Thermo ESCALAB 250XI).

3. Results and Discussion

Figure 1(a) shows the SEM image of the developed AgGeSbTe film, exhibiting a clear and uniform surface morphology. Figure 1(a1) shows the AFM image of the exposed sample, presenting clear but quite shallow line structures. Figure 1(b) displays the cross-section profile of the developed film, where the exposed region is higher compared to the as-deposited region, and the height difference reaches 62 nm at the developing time of 1 min, showing a negative-tone characteristic. The magnified SEM image of Fig. 1(a2) reveals the smooth etched lines with low line edge roughness. The etching rate difference is as high as 62 nm/min, where the etching rate is defined as the ratio of etching height to time, and the etching rate difference is defined as the difference between etching rate of the exposure region and that of the non-exposed region. The high difference of etching rate means high etching selectivity of AgGeSbTe resist at CHF_3/O_2 mixed gases. The TEM cross-section image of Fig. 1(c) reveals the steep sidewall (86°) without obvious lateral corrosion.

Figure 2(a) shows the influence of etching power on linewidth and etching height. It is found that the linewidth is hardly changed, while the etching height increases gradually with etching power. This is mainly due to the higher power providing more energy for active ions and making the etching rate larger. When the power reaches 240 W, the etching height increases to about 250 nm, which is nearly the same as the thickness of AgGeSbTe film. Figure 2(b) shows the influence of developing time on linewidth and etching height. It is revealed that the linewidth is hardly changed, whereas the etching height increases firstly and then reduces with the increasing developing time. When the developing time is 2 min, the etching height reaches the maximum. The reduction of height is due to the weakened etching resistance and increased etching rate of the exposed region after 3 min. Figure 2(c) depicts the influence of laser energy on linewidth and etching height, respectively. One can see the increment of linewidth and height when the laser energy becomes larger. The reason is that the generated heat becomes

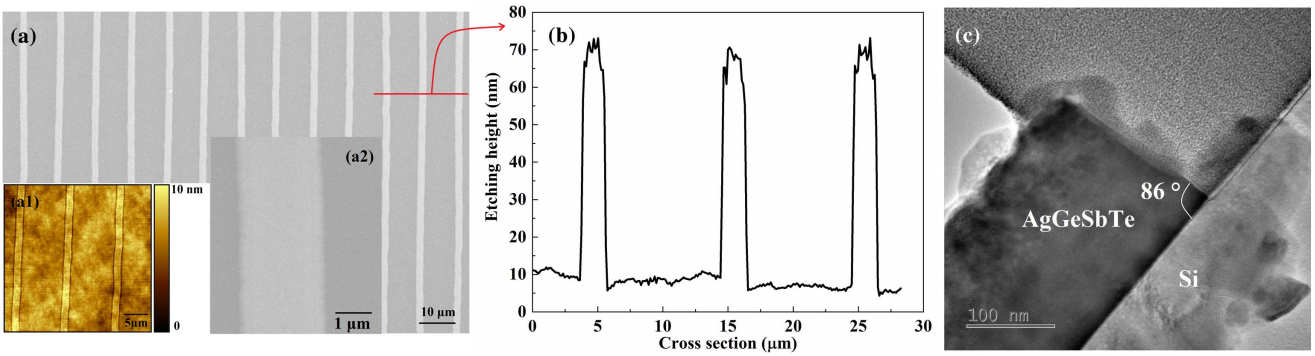

Fig. 1. (a) SEM image; (a1) AFM image of the exposed sample, (a2) magnified SEM image of developed sample; (b) corresponding cross-section curve; and (c) TEM cross-section image of AgGeSbTe heat-mode resist. For (a) and (b), the laser energy is 0.7×10^3 mJ/cm^2. The gas flow ratio of CHF_3/O_2 is 60/2. The etching power is 200 W, and the chamber pressure is 50 mTorr with the time of 1 min. For (c), the laser energy is 1.2×10^3 mJ/cm^2, and the etching time is 3 min.

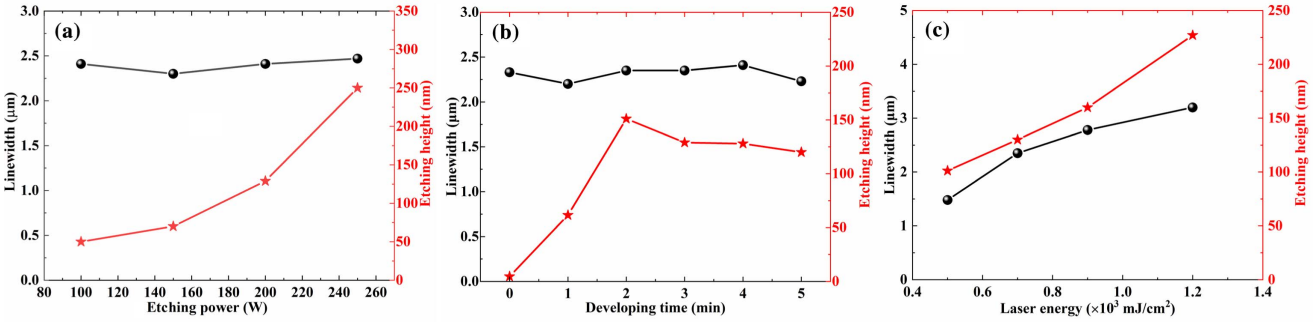

Fig. 2. Dependence of (a) etching power, (b) developing time, and (c) laser power on linewidth and height of grating structures. For (a), the laser energy is 0.8×10^3 mJ/cm^2. The gas flow ratio of CHF_3/O_2 is 60/2, and the chamber pressure is 50 mTorr with the time of 4 min. For (b), the laser energy is 0.7×10^3 mJ/cm^2. The gas flow ratio of CHF_3/O_2 is 60/2, and the etching power is 200 W with the chamber pressure of 50 mTorr. For (c), the gas flow ratio of CHF_3/O_2 is 60/2, the etching power is 200 W, the chamber pressure is 50 mTorr, and the developing time is 3 min. The thickness of AgGeSbTe film is 250 nm.

more and more as the laser energy increases, which enhances the thermal diffusion in the horizontal and vertical directions[21].

To more clearly understand the physical mechanism where laser energy influences the linewidth and height, the thermal distribution of AgGeSbTe resist is analyzed by COMSOL software with the finite element method. It is noted that the optical and thermal parameters of GeSbTe films are utilized due to the lack of relative parameters of AgGeSbTe[21]. The laser pulse width is set to 50 ns to achieve the crystallization of AgGeSbTe films based on the fast crystallization speed of phase-change material[1]. Figure 3(a) displays the relationship between sheet resistance and temperature. The slow reduction of sheet resistance is related to the semiconductor behavior. However, the dramatic reduction of sheet resistance at 290°C–300°C is ascribed to the phase-change process of thin film. Thus, the phase-change temperature of AgGeSbTe film is 290°C via the intersection of the tangent. Figure 3(b) shows the temperature field of the resist at fixed laser energy, showing the thermal

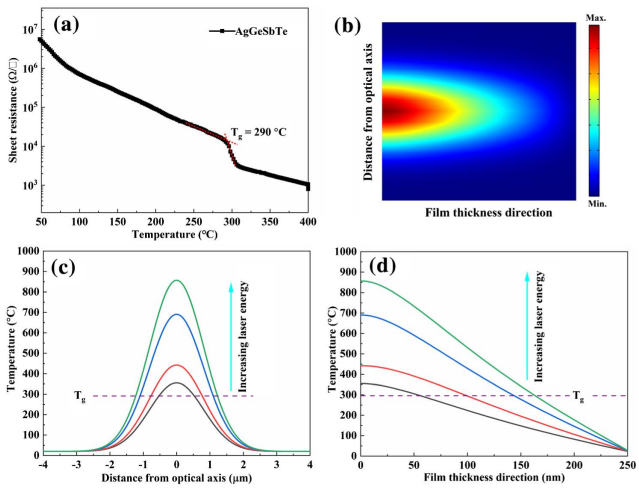

Fig. 3. (a) Relationship between sheet resistance and temperature in AgGeSbTe thin film. (b) Thermal field distribution of heat-mode resist in thickness direction. (c) and (d) Temperature profiles in radius and thickness directions, respectively.

diffusions in both thickness and radius directions. Figures 3(c) and 3(d) display the temperature profiles with different laser energies in the radius and thickness directions, respectively. One can see that the diameter and penetration depth of the heat spot both increase with the laser energy. This tendency is in good consistence with the result of Fig. 2(c).

To further understand the structural evolution after laser exposure, X-ray diffraction (XRD) patterns of AgGeSbTe films are obtained in Fig. 4(a), showing the amorphous nature in the as-deposited state, while phase separation happens and crystalline phases of Ge, Sb, and AgTe occur after laser exposure. The bonding environment is also investigated by Raman and XPS spectra [Figs. 4(b) and 4(c)]. One can see from Fig. 4(b) that the as-deposited sample presents a broad Raman peak at 50–200 cm^{-1}, whereas the exposed sample exhibits two Raman peaks at 118 cm^{-1} and 151 cm^{-1}, respectively. The main peak at 151 cm^{-1} is due to the Sb-Te vibrations of $SbTe_3$ units, or it originated from the defective octahedron of Sb atoms[22]. Another peak at 118 cm^{-1} is due to the A_1 vibration mode of $GeTe_{4-n}Ge_n$ ($n = 1$, 2) corner sharing tetrahedron[22]. In Fig. 4(c), Gaussian fitting is also performed to obtain more structural information. In the as-deposited state, the binding energies at 30.11 eV and 30.71 eV correspond to octahedra, defective octahedra (i.e., $Ge^{oct+def-oct}$), and tetrahedra, pyramid structures (i.e., $Ge^{tet+pyr}$), respectively[22]. After laser exposure, the peak of $Ge^{oct+def-oct}$ is enhanced, while the peak of $Ge^{tet+pyr}$ decreases, indicating the generation of the Ge atom arrangement. In addition, the energy peaks all shift to higher directions after laser exposure. It is well known that the electronegativity of Ag (1.93) is lower than that of Ge (2.01), Sb (2.05), and Te (2.1), which will lead to the reduced binding energy for Ge, Sb, and Te when bonding to Ag[23,24]. However, the increased binding energies of Ge 3d, and Sb 4d levels after laser exposure indicate the generation of Ge-Ge and Sb-Sb bonds. Overall, the structural difference between as-deposited and exposed states is the basis of etching selectivity in AgGeSbTe resist.

In the previous research[20], $CrSb_2Te$ thin film acted as a positive resist, while AgGeSbTe thin film can act as a negative resist in this work. The positive/negative-tone characteristic of resist is

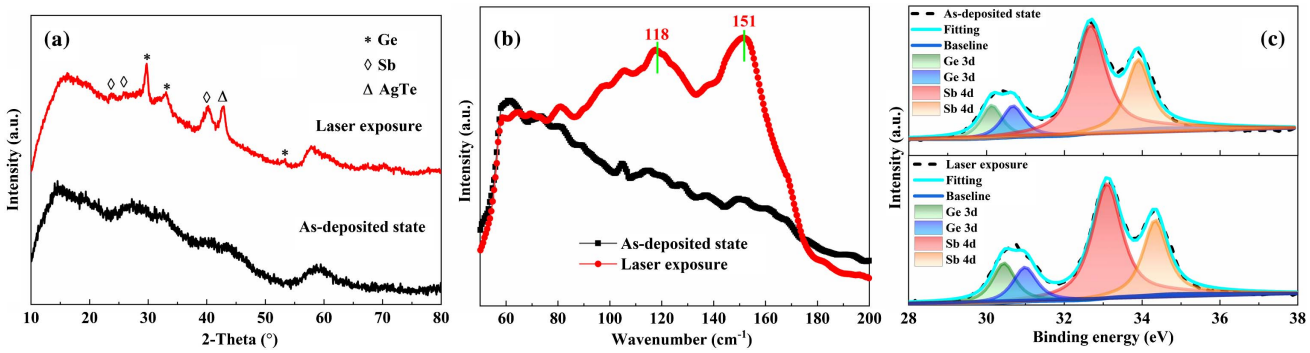

Fig. 4. (a) XRD patterns, (b) Raman data, and (c) XPS profiles of the as-deposited and laser-exposed AgGeSbTe films, where the exposed energy is 0.7×10^3 mJ/cm^2.

closely related to its structural difference, that is, Cr doping leads to the phase separation of Sb_2Te and the occurrence of Sb crystals, while the Ag doping results in the phase separation of GeSbTe and the generation of Ge, Sb, and AgTe crystals after laser irradiation. Under CHF_3/O_2 mixed gases, the precipitated Sb crystal of $CrSb_2Te$ is readily broken compared with the as-deposited state, causing the positive-tone characteristic. However, the precipitated Ge and AgTe crystals of AgGeSbTe are difficult to be etched owing to their higher mechanical strength compared with the as-deposited state. Thus, the negative-tone characteristic is obtained under the same etching gases. The positive/negative-tone mechanism of resist is very complicated and will be further investigated in detail in the future.

Etching resistance of AgGeSbTe resist is further evaluated via SF_6 and Ar mixed gases, where the Si substrate is adopted, and the results are shown in Fig. 5. In Fig. 5(a), the height of AgGeSbTe resist after development is 220 nm, and the non-exposed region is completely removed, as shown in the inset of Fig. 5(a). After further etching by SF_6 and Ar mixed gases for 5 min, the height difference (ΔH) reaches 940 nm, which contains the etching height of Si and the residual thickness of AgGeSbTe resist [Fig. 5(b)]. In order to accurately distinguish the thickness of them, pure Si is also etched under the same condition, as displayed in Fig. 5(c). One can see that the etching height (ΔH) of Si is 760 nm at the time of 5 min with the etching rate of as high as 152 nm/min. Hence, the residual thickness of AgGeSbTe resist is 180 nm, and the AgGeSbTe resist is etched by 40 nm with the etching rate of as low as 8 nm/min. Therefore, the etching selectivity of Si to AgGeSbTe resist reaches 19. Results indicate that the AgGeSbTe resist possesses good etching resistance.

4. Conclusion

In summary, an AgGeSbTe thin film is proposed as a negative heat-mode resist for dry lithography. It is found that the resist possesses high etching selectivity with the etching rate difference of as high as 62 nm/min. The etched sidewall is steep without the obvious lateral corrosion. The influences of laser energy, etching power, and developing time on linewidth and developing height are also investigated. The underlying physical mechanism is further analyzed. Results of XRD, Raman, and XPS profiles indicate that laser exposure induces the phase separation of AgGeSbTe resist and the occurrence of Ge, Sb, and AgTe crystals, which is the basis of etching selectivity. Besides, the

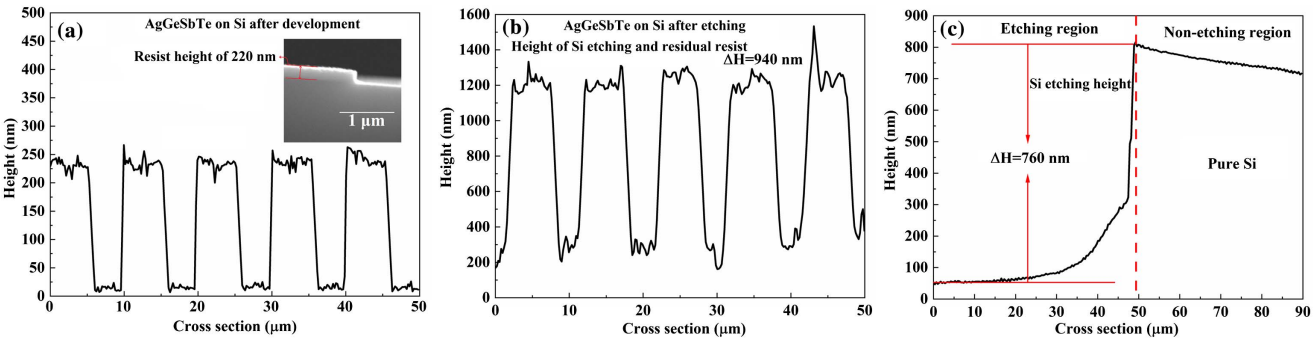

Fig. 5. AFM cross-section profiles of (a) development, (b) etching of AgGeSbTe resist on Si substrate, and (c) etching of the pure Si, where the exposed energy is 1.2×10^3 mJ/cm^2. For development of (a), the gas flow ratio of CHF_3/O_2 is 60/2. The etching power is 200 W, and the chamber pressure is 50 mTorr with the developing time of 3 min. Inset of (a) is SEM cross-section image of the developed sample. For Si etching of (b) and (c), the gas flow ratio of SF_6/Ar is 15/35. The etching power is 150 W, and the chamber pressure is 50 mTorr with the etching time of 5 min.

AgGeSbTe resist possesses good etching resistance with the etching selectivity of Si to AgGeSbTe resist of as high as 19. The proposed AgGeSbTe resist may have potential applications in micro/nano fabrications.

Acknowledgement

The work was supported by the National Natural Science Foundation of China (Nos. 21773291, 61904118, and 22002102), Natural Science Foundation of Jiangsu Province (Nos. BK20190935 and BK20190947), Natural Science Foundation of the Jiangsu Higher Education Institutions of China (No. 19KJA210005), and Jiangsu Key Laboratory for Environment Functional Materials.

†These authors contributed equally to this work.

References

1. J. Wei, *Laser Heat-Mode Lithography: Principle and Methods* (Springer, 2019).
2. A. S. Basu, S. McNamara, and Y. B. Gianchandani, "Scanning thermal lithography: maskless, submicron thermochemical patterning of photoresist by ultracompliant probes," J. Vac. Sci. Technol. B **22**, 3217 (2004).
3. W. C. Tian, Y. H. Ho, C. H. Chen, and C. Y. Kuo, "Sensing performance of precisely ordered TiO_2 nanowire gas sensors fabricated by electron-beam lithography," Sensors **13**, 865 (2013).
4. S. Wang, Z. Zhou, B. Li, C. Wang, and Q. Liu, "Progresses on new generation laser direct writing technique," Mater. Today Nano **16**, 100142 (2021).
5. J. Chen, G. Chen, and Q. Zhan, "Self-aligned fiber-based dual-beam source for STED nanolithography," Chin. Opt. Lett. **19**, 072201 (2021).
6. T. Yang, H. Lin, and B. Jia, "Ultrafast direct laser writing of 2D materials for multifunctional photonics devices [Invited]," Chin. Opt. Lett. **18**, 023601 (2020).
7. T. Jiang, S. Gao, Z. Tian, H. Zhang, and L. Niu, "Fabrication of diamond ultrafine structures by femtosecond laser," Chin. Opt. Lett. **18**, 101402 (2020).
8. Y. Usami, T. Watanabe, Y. Kanazawa, K. Taga, H. Kawai, and K. Ichikawa, "405 nm laser thermal lithography of 40 nm pattern using super resolution organic resist material," Appl. Phys. Express **2**, 126502 (2009).
9. B. J. Zeng, J. Z. Huang, R. W. Ni, N. N. Yu, W. Wei, Y. Z. Hu, Z. Li, and X. S. Miao, "Metallic resist for phase-change lithography," Sci. Rep. **4**, 5300 (2014).
10. T. Luo, Z. Li, Q. He, and X. Miao, "Pr-based metallic glass films used as resist for phase-change lithography," Opt. Express **24**, 5754 (2016).
11. H. Xi, Q. Liu, Y. Tian, Y. Wang, S. Guo, and M. Chu, "$Ge_2Sb_{1.5}Bi_{0.5}Te_5$ thin film as inorganic photoresist," Opt. Mater. Express **2**, 461 (2012).
12. H. Xi, Q. Liu, Y. Tian, S. Guo, M. Cu, and G. Zhang, "The study on SiO_2 pattern fabrication using $Ge_{1.5}Sn_{0.5}Sb_2Te_5$ as resists," J. Nanosci. Nanotechnol. **13**, 829 (2013).
13. Y. Meng, J. K. Behera, Z. Wang, J. Zheng, J. Wei, L. Wu, and Y. Wang, "Nanostructure patterning of C-Sb_2Te_3 by maskless thermal lithography using femtosecond laser pulses," Appl. Surf. Sci. **508**, 145228 (2020).
14. J. Wei, K. Zhang, T. Wei, Y. Wang, Y. Wu, and M. Xiao, "High-speed maskless nanolithography with visible light based on photothermal localization," Sci. Rep. **7**, 43892 (2017).
15. Z. Wang, J. Zheng, G. Chen, K. Zhang, T. Wei, Y. Wang, X. Liu, Z. Mo, T. Gao, M. Wen, and J. Wei, "Laser-assisted thermal exposure lithography: arbitrary feature sizes," Adv. Eng. Mater. **23**, 2001468 (2021).
16. K. Zhang, Z. Wang, G. Chen, J. Zheng, Z. Mo, Y. Wang, and J. Wei, "Laser heat-mode patterning with improved aspect-ratio," Mat. Sci. Semicon. Proc. **134**, 106018 (2021).
17. G. Chen, J. Zheng, Z. Wang, K. Zhang, Z. Mo, X. Liu, T. Gao, Y. Wang, and J. Wei, "Fabrication of micro/nano multifunctional patterns on optical glass through chalcogenide heat-mode resist AgInSbTe," J. Alloys Compd. **867**, 158988 (2021).
18. Y. Q. Huang, R. Huang, Q. L. Liu, C. C. Zheng, J. Q. Ning, Y. Peng, and Z. Y. Zhang, "Realization of III-V semiconductor periodic nanostructures by laser direct writing technique," Nanoscale Res. Lett. **12**, 12 (2017).
19. Z. Wang, K. Zhang, G. Chen, Z. Zhu, Y. Wang, and J. Wei, "A metal lift-off process through hyperbolic undercut of laser heat-mode lithography," Mater. Lett. **264**, 127344 (2020).
20. T. Wei, B. Liu, W. Li, Y. Ling, J. Hu, Q. Liu, M. Cheng, and J. Wei, "$CrSb_2Te$ thin film as a dry resist and its etching mechanism for lithography application," Mater. Chem. Phys. **266**, 124558 (2021).
21. T. Wei, J. Wei, Y. Wang, and L. Zhang, "Manipulation and simulations of thermal field profiles in laser heat-mode lithography," J. Appl. Phys. **122**, 223107 (2017).
22. J. H. Han, K.-S. Jeong, M. Ahn, D.-H. Lim, W. J. Yang, S. Jong Park, and M.-H. Cho, "Modulation of phase change characteristics in Ag-incorporated $Ge_2Sb_2Te_5$ owing to changes in structural distortion and bond strength," J. Mater. Chem. C **5**, 3973 (2017).
23. S. Hwang, H. Park, D. Kim, H. Lim, C. Lee, J. H. Han, Y.-K. Kwon, and M.-H. Cho, "Ultra-low energy phase change memory with improved thermal stability by tailoring the local structure through Ag doping," ACS Appl. Mater. Inter. **12**, 37285 (2020).
24. T. Wei, Q. Wang, S. Song, Z. Song, and B. Liu, "Reversible phase-change characteristics and structural origin in Cr doped $Ge_2Sb_2Te_5$ thin films," Thin Solid Films **716**, 138434 (2020).